PERGAMON

Solid-State Electronics 43 (1999) 1723–1735

SOLID-STATE ELECTRONICS

Numerical analysis of the detectivity in n^+–n–p and p^+–p–n GaInAsSb infrared detectors

Yuan Tian*, Baolin Zhang, Tianming Zhou, Hong Jiang, Yixin Jin

Changchun Institute of Physics, Chinese Academy of Sciences, Changchun 130021, People's Republic of China

Accepted 29 January 1999

Abstract

In this paper, the detectivity for n^+–n–p and p^+–p–n GaInAsSb infrared detectors in both the front- and backside illuminated cases are calculated and analyzed, respectively. The influence of the carrier concentration and width in each layer, as well as the surface recombination velocities at different surfaces of the detectors are considered. It is indicated that high R_0A dose not guarantee the high detectivity because the quantum efficiency combines with the R_0A to determine the behavior of D^*. On the base of the calculations, it is observed that the different material parameters are required for the optimum D^* in the different structures with the different directions of the light injected.

1. Introduction

Antimonide-based semiconductor materials are receiving increased attention due to their usefulness for photonic devices, particularly emitters and detectors in 2–5 μm region of the spectrum [1,2]. In these materials, GaInAsSb quaternary solid solutions grown lattice matched to GaSb substrates are attractive candidate materials for opto-electronic devices in the near- and mid-infrared wavelength range. These devices can be used for environmental monitoring, optical fiber communication and infrared imaging systems [3–5]. Also GaInAsSb quaternary alloys are of great interest for creation of light sources and photodetectors in 2–5 μm [6–8]. There have been theoretical analysis on n–p homojunction GaInAsSb infrared detectors [9,10]. However, most detectors are fabricated in three-layer structures, in which the surface influence can be effectively reduced by the heavily-doped epitaxial layers [11,12]. Although the zero-bias resistance–area product, R_0A, of GaInAsSb infrared detectors, on the base of material parameters, has been reported [13], the high R_0A does not automatically guarantee the high detectivity D^*, because of the effect of the quantum efficiency η on D^*, which is another important parameter to decide the properties of detectors. In this paper, the numerical analysis of the quantum efficiency (η) and the detectivity (D^*) are discussed in both n^+–n–p and p^+–p–n GaInAsSb infrared detectors, for both front- and backside illuminated cases. Since R_0A is independent on the light incident light, whether the detector is front- or backside illuminated cases does not affect R_0A.

2. Theoretical model

The detector structures of p^+–p–n and n^+–n–p GaInAsSb are shown in Fig. 1. The heavily-doped

* Corresponding author. Tel.: +86-431-5952215; fax: +86-431-5955378.

E-mail address: snmocvd@public.cc.jl.cn (Y. Tian)

0038-1101/99/$ - see front matter
PII: S0038-1101(99)00049-0

Nomenclature

S_p	Surface recombination velocity in n- (or n^+-)side	t	Width in n-side
t_{n^+}	Width in n^+-side	l_p	Hole diffusion length in n-side
n^+	Electron concentration in n^+-side	D_p	Hole diffusion coefficient in n-side
l_{pn^+}	Hole diffusion length in n^+-side	W_{np}	Width of depletion region in n–p junction
D_{pn^+}	Hole diffusion coefficient in n^+-side	W_{nn}	Width of depletion region in n^+–n junction
S_{nn}	Interface recombination velocity in n^+–n junction	W_{pp}	Width of depletion region in p^+–p junction
p^+	Hole concentration in p^+-side	W_n	Width in n-side depletion region of n–p junction
d_{p^+}	Width in p^+-side	W_p	width in p-side depletion region of n–p junction
l_{ep^+}	Electron diffusion length in p^+-side	K	Boltzmann's constant
D_{ep^+}	Electron diffusion coefficient in p^+-side	T	Detector temperature
S_{pp}	Interface recombination velocity in p^+–p junction	q	Electronic charge
p	Hole concentration in p-side	σ	Capture cross section
d	Width in p-side	N_f	Trap density
l_e	Electron diffusion length in p-side	E_g	GaInAsSb energy bandgap
D_e	Electron diffusion coefficient in p-side		
n	Electron concentration in n-side		

layer surface is defined as the frontside and the other layer surface is the backside. The figure of merit used to characterize the sensitivity of infrared detectors is the detectivity D^*, which is related with R_0A and η,

$$D* = \frac{\lambda\eta q}{hc}\left(\frac{R_0A}{4KT}\right)^{1/2}$$

λ is the incident light wavelength, which is assumed to be 2.48 μm. R_0A and its related parameters have been evaluated in a previous paper [13]. The detailed calculation of η and D^* for front- and backside illuminated cases in n^+–n–p and p^+–p–n GaInAsSb infrared detectors is given in this paper.

2.1. Quantum efficiency in an n^+–n–p structure

According to Dhar's report for an n^+–n–p structure [14], at a wavelength λ where the absorption coefficient is α, the contribution to the internal quantum efficiency η of n^+, n, depletion and p layers for the front- and backside illuminated cases is shown as follows.

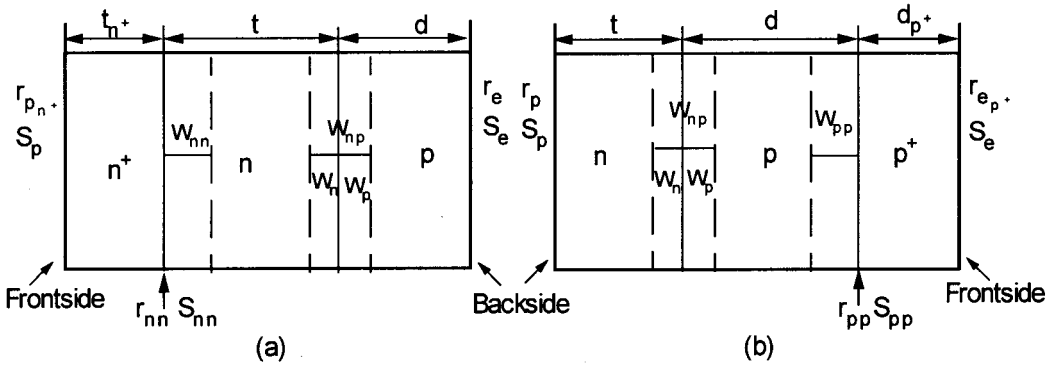

Fig. 1. The two structures of a GaInAsSb detector.

2.1.1. Frontside illuminated case

(1) Quantum efficiency in the n^+ region:

$$\eta_{n^+} = \frac{\alpha L_{pn^+}}{\alpha^2 L_{pn^+}^2 - 1}\left[A\sinh\left(\frac{t_{n^+}}{L_{pn^+}}\right) + B\cosh\left(\frac{t_{n^+}}{L_{pn^+}}\right) + \alpha L_{pn^+}e^{-\alpha t_{n^+}}\right]$$

$$B = \gamma_p A - (\gamma_p + \alpha L_{pn^+})$$

$$A = \frac{(\gamma_p + \alpha L_{pn^+})\left[\cosh\left(\frac{t_{n^+}}{L_{pn^+}}\right) - \gamma_{nn}\sinh\left(\frac{t_{n^+}}{L_{pn^+}}\right)\right] - (\gamma_{nn} + \alpha L_{pn^+})e^{-\alpha t_{n^+}}}{\left[\gamma_p\cosh\left(\frac{t_{n^+}}{L_{pn^+}}\right) + \sinh\left(\frac{t_{n^+}}{L_{pn^+}}\right)\right] - \gamma_{nn}\left[\cosh\left(\frac{t_{n^+}}{L_{pn^+}}\right) + \gamma_p\sinh\left(\frac{t_{n^+}}{L_{pn^+}}\right)\right]}$$

(2) Quantum efficiency in the n region:

$$\eta_n = \frac{\alpha L_{pn}}{\alpha^2 L_{pn}^2 - 1}\left[C\sinh\left(\frac{t_{n^+}^{+t-w_n}}{L_{pn}}\right) - D\cosh\left(\frac{t_{n^+}^{+t-w_n}}{L_{pn}}\right) - \alpha L_{pn}e^{-\alpha(t_{n^+}+t-w_n)}\right]$$

$$C = \frac{D\sinh\left(\frac{t_{n^+}+t-w_n}{L_{pn}}\right) - e^{-\alpha(t_{n^+}+t-w_n)}}{\cosh\left(\frac{t_{n^+}+t-w_n}{L_{pn}}\right)}$$

$$D = \frac{e^{-\alpha(t_{n^+}+t-w_n)}\left[\gamma_{nn}\cosh\left(\frac{t_{n^+}}{L_{pn}}\right) - \sinh\left(\frac{t_{n^+}}{L_{pn}}\right)\right] - (\gamma_{nn} + \alpha L_{pn})e^{-\alpha t_{n^+}}\cosh\left(\frac{t_{n^+}+t-w_n}{L_{pn}}\right)}{\cosh\left(\frac{t-w_n}{L_{pn}}\right) + \gamma_{nn}\sinh\left(\frac{t-w_n}{L_{pn}}\right)}$$

(3) Quantum efficiency in the depletion region:

$$\eta_{dr} = e^{-\alpha(t_{n^+}+t-w_n)} - e^{-\alpha(t_{n^+}+t+w_p)}$$

(4) Quantum efficiency in the p region:

$$\eta_p = \frac{\alpha L_{np}}{\alpha^2 L_{np}^2 - 1}e^{-\alpha(t_{n^+}+t+w_p)}\left(\alpha L_{np} - \frac{(\alpha L_{np} - r_e)e^{-\alpha(d-w_p)} + \left[r_e\cosh\left(\frac{d-w_p}{L_{np}}\right) + \sinh\left(\frac{d-w_p}{L_{np}}\right)\right]}{r_e\sinh\left(\frac{d-w_p}{L_{np}}\right) + \cosh\left(\frac{d-w_p}{L_{np}}\right)}\right)$$

2.1.2. Backside illuminated case

(1) Quantum efficiency in the p region:

$$\eta_p = \frac{\alpha L_{np}}{\alpha^2 L_{np}^2 - 1}\left(\frac{\alpha L_{np} + r_e - e^{-\alpha(d-w_p)}\left[r_e\cosh\left(\frac{d-w_p}{L_{np}}\right) + \sinh\left(\frac{d-w_p}{L_{np}}\right)\right]}{r_e\sinh\left(\frac{d-w_p}{L_{np}}\right) + \cosh\left(\frac{d-w_p}{L_{np}}\right)} - \alpha L_{np}e^{-\alpha(d-w_p)}\right)$$

(2) Quantum efficiency in the depletion region:

$$\eta_{dr} = e^{-\alpha(d-w_p)} - e^{-\alpha(d+w_n)}$$

(3) Quantum efficiency in the n region:

$$\eta_n = \frac{\alpha L_{pn}}{\alpha^2 L_{pn}^2 - 1}\left[A\sinh\left(\frac{d+w_n}{L_{pn}}\right) + B\cosh\left(\frac{d+w_n}{L_{pn}}\right) + \alpha L_{pn}e^{-\alpha(d+w_n)}\right]$$

$$A = \frac{e^{-\alpha(d+w_n)} - B\sinh\left(\frac{d+w_n}{L_{pn}}\right)}{\cosh\left(\frac{d+w_n}{L_{pn}}\right)}$$

$$B = \frac{(\gamma_{nn} - \alpha L_{pn})e^{-\alpha(d+t)}\cosh\left(\frac{d+w_n}{L_{pn}}\right) - e^{-\alpha(d+t)}\left[\sinh\left(\frac{d+t}{L_{pn}}\right) + \gamma_{nn}\cosh\left(\frac{d+t}{L_{pn}}\right)\right]}{\cosh\left(\frac{t-w_n}{L_{pn}}\right) + \gamma_{nn}\sinh\left(\frac{t-w_n}{L_{pn}}\right)}$$

(4) Quantum efficiency in the n^+ region:

$$\eta_{n^+} = \frac{\alpha L_{pn^+}}{\alpha^2 L_{pn^+}^2 - 1}\left[C\sinh\left(\frac{d+t}{L_{pn^+}}\right) + D\cosh\left(\frac{d+t}{L_{pn^+}}\right) + \alpha L_{pn^+}e^{-\alpha(d+t)}\right]$$

$$C = \frac{e^{-\alpha(d+t+t_{n^+})}(\gamma_p - \alpha L_{pn^+}) - D\left[\cosh\left(\frac{d+t+t_{n^+}}{L_{pn^+}}\right) + \gamma_p\sinh\left(\frac{d+t+t_{n^+}}{L_{pn^+}}\right)\right]}{\sinh\left(\frac{d+t+t_{n^+}}{L_{pn^+}}\right) + \gamma_p\cosh\left(\frac{d+t+t_{n^+}}{L_{pn^+}}\right)}$$

$$D = \frac{e^{-\alpha(d+t)}(\gamma_{nn} - \alpha L_{pn^+})\left[\sinh\left(\frac{d+t+t_{n^+}}{L_{pn^+}}\right) + \gamma_p\cosh\left(\frac{d+t+t_{n^+}}{L_{pn^+}}\right)\right] - e^{-\alpha(d+t+t_{n^+})}(\gamma_p - \alpha L_{pn^+})\left[\sinh\left(\frac{d+t}{L_{pn^+}}\right) + \gamma_{nn}\cosh\left(\frac{d+t}{L_{pn^+}}\right)\right]}{\left[\gamma_p\cosh\left(\frac{t_{n^+}}{L_{pn^+}}\right) + \sinh\left(\frac{t_{n^+}}{L_{pn^+}}\right)\right] - \gamma_{nn}\left[\cosh\left(\frac{t_{n^+}}{L_{pn^+}}\right) + \gamma_p\sinh\left(\frac{t_{n^+}}{L_{pn^+}}\right)\right]}$$

In the above two groups of equation, the symbols of D, L and r are defined by $D = KT\mu/q$, $L = (D\tau)^{1/2}$, $r = LS/D$.

2.2. Quantum efficiency in a p^+–p–n structure

The expressions of the quantum efficiency for the front- and backside illuminated cases in a p^+–p–n structure are the same as those in an n^+–n–p structure, but the parameters in an n^+–n–p structure should be exchanged to the corresponding ones in a p^+–p–n structure, which are shown as following,

$$n^+\to p^+;L_{pn^+}\to L_{np^+};t_{n^+}\to d_{p^+};r_p\to r_e;r_{nn}\to r_{pp};n\to p;L_{pn}\to L_{np};t\to d;W_n\to W_p;L_{np}\to L_{pn};W_p\to W_n;r_e\to r_p;d\to t;p\to n$$

The parameters before the arrow are the ones in the n^+–n–p structure and those after the arrow are in the p^+–p–n structure.

3. Results and discussion

The calculations have been performed on n^+–n–p and p^+–p–n $Ga_{0.8}In_{0.2}As_{0.19}Sb_{0.81}$ infrared detectors operated at 300 K and 2.5 μm wavelength. The results of this model are displayed mostly in the form of plots of η and D^* versus the carrier concentrations and material widths, for front- and backside illuminated cases. The basic parameters are listed in Table 1 and related parameters have been shown in Ref. [9].

3.1. The detectivity in a p^+–p–n structure

Fig. 2 shows the quantum efficiency (η) and its components as functions of p- and n-side carrier concentrations with other parameters in Table 1 keeping constants, in the backside illuminated case. There are some characters in Fig. 2: (1) η is mainly dominated by the p-side component, η_p; (2) the quantum efficiency in the depletion region, η_{dr}, decreases with increasing the p- and n-side carrier concentrations, due to the decreasing of the width in the depletion region; (3) the p-side quantum efficiency η_p increases with increasing the p-side carrier concentration (p) while the n-side quantum efficiency η_n decreases with increasing the n-side carrier concentration (n). In addition, in Fig. 2(a) the quantum efficiency in the p^+-side (η_{p^+}) markedly rises with increasing p and becomes the main contribution to η in $p > 5\times10^{17}$ cm^{-3}, which makes η strongly increased in this range. In Fig. 2(b), η_n and η_{dr} in $n < 10^{17}$ cm^{-3} are large enough to improve η, while in $n > 10^{17}$ cm^{-3}, η is mainly contributed by η_p and a little by η_{p^+}. Due to η_n and η_{dr} decreasing, η decreases with increasing n.

Table 1
Basic parameters for the n^+–n–p and p^+–p–n structures

Basic parameters	T = 300 K, x = 0.8, $N_f = 10^{14}$ cm^{-3}, $\sigma_s = 10^{-15}$ cm^2					
	n^+–n–p structure			p^+–p–n structure		
	n^+-region	n-region	p-region	p^+-region	p-region	n-region
Carrier concentration (cm^{-3})	5×10^{18}	10^{18}	10^{17}	10^{18}	10^{17}	10^{18}
Width (μm)	0.5	2	5	0.5	5	2
Mobility (cm^2/V s)	1000	1000	240	240	240	1000
Surface recombination velocity (m/s)	0		0	0		0

Fig. 3 shows the dependence of the detectivity (D^*) in the backside illuminated case on the p-side carrier concentration (p) with the p^+-side carrier concentration (p^+), the width (d_{p^+}) and the surface recombination velocity (S_e) as parameters, under the condition of other parameters in Table 1 keeping constant. Compared to the report in Ref. [13], except that the shape of D^* is similar to R_0A with $p^+ = 10^{21}$ cm^{-3} in Fig. 3(a) and $S_e = 10^8$ m/s in Fig. 3(c), D^* is determined by η and its shape is similar to η in Fig. 2(a). In addition, η and R_0A have the similar various trend with the influence of the p^+-side carrier concentration and the surface recombination velocity. That is, increasing p^+ and S_e will simultaneously reduce R_0A and η, therefore D^* decreases. The relation between D^* and d_{p^+} has a little difference from D^* related with p^+ and S_e. With the change of d_{p^+}, D^* appears a intersection at p near to 10^{17} cm^{-3}. In $p < 10^{17}$ cm^{-3}, D^* is determined by R_0A and it decreases with increasing d_{p^+} because of the same variety of R_0A, while in $p > 10^{17}$ cm^{-3}, D^* first increases with increasing d_{p^+} and then the value of D^* at $d_{p^+} = 0.5$ μm far exceeds

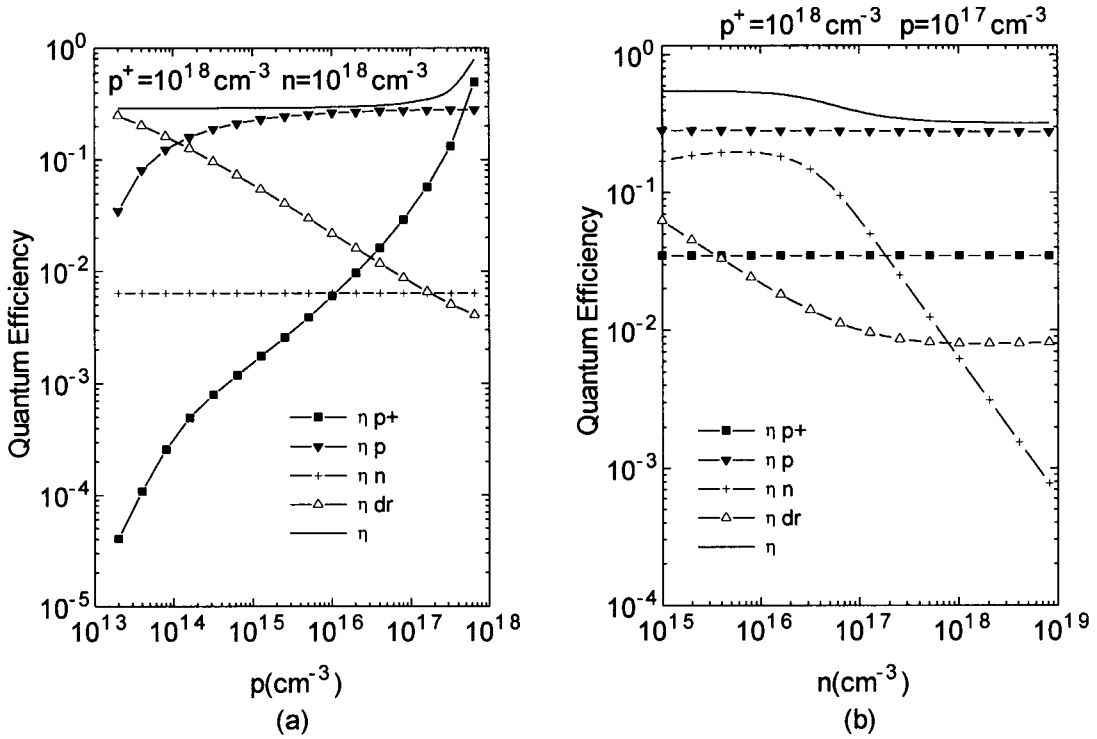

Fig. 2. The dependence of η and its components on (a) the p-side carrier concentration (p) and (b) the n-side carrier concentration (n) for the p^+–p–n structure in the backside illuminated case.

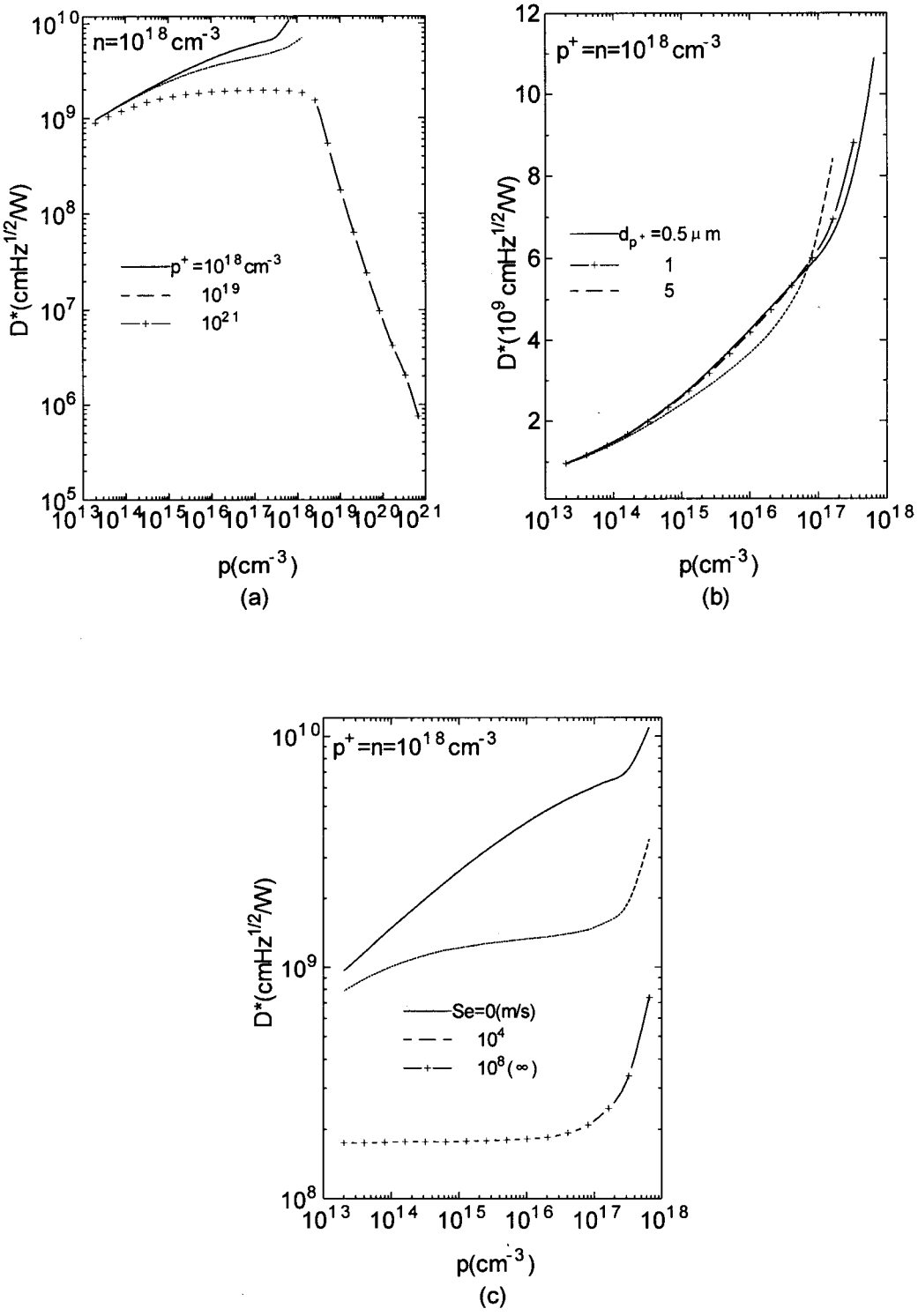

Fig. 3. The dependence of D^* on the p-side carrier concentration (p) with the p^+-side (a) carrier concentration (p^+); (b) width (d_{p^+}) and (c) surface recombination velocity (S_e) as parameters for the p^+–p–n structure in the backside illuminated case.

those at $d_{p^+} > 0.5$ μm, which is the same as η. Fig. 3 indicates that D^* is the result of the joint influence of R_0A and η. With the variety of the p-side width, D^* is similar to that in Fig. 3(b), in which the intersection appears and moves to a higher p. In this case, D^* is also determined by the R_0A and η.

In Fig. 4 and Fig. 5, the detectivity is depicted as a function of the n-side carrier concentration (n), with the n-side width (t) and the surface recombination velocity (S_p) as parameters, in the back- and frontside illuminated cases respectively. Compared the two figures with each other, the results are completely different.

In the backside illuminated case, the light incident from the n-side surface is first through the n region and then reaches the depletion region, in which η_n and η_{dr} related with t and S_p will contribute to η in $n < 10^{17}$ cm^{-3} as shown in Fig. 2(b). Moreover from the expressions for the quantum efficiency in the backside illuminated case, we know that the n-side width is also one of the major parameters to affect the quantum efficiency in the p and p^+ regions. Increasing t will markedly reduce η_p and η_{p^+} and at the same time η decreases. On the other hand, D^* is determined by η. Therefore the parameters in the n region have strong influence on D^* as shown in Fig. 4. With increasing t and S_p, D^* remarkably deceases and its peak moves to low n with high t in Fig. 4(a) and to high n with high S_p in Fig. 4(b), respectively.

However, in the frontside illuminated case, D^* and its shape are controlled by R_0A and η through t and S_p only has a little influence on D^* in $n < 10^{17}$ cm^{-3}. As for the backside illuminated case, η_n and η_{dr} for the frontside illuminated case improve η in $n < 10^{17}$ cm^{-3}. But the intensity of the light incident form the p^+-side surface is weakened exponentially. When the light through the n region reaches the depletion region, η_n and η_{dr} are so low that only has a little influence on η. Meanwhile η_p and η_{p^+} keep constants with the change of n because they are not related with the n-side parameters. These results in this case determine that η is almost not influenced by t and S_p. But R_0A with the change of n rises up and becomes the main contribution to D^*. In the frontside illuminated case, D^* with the change of the p^+- and p-side parameters are similar to but slightly higher than the one in the backside illuminated case, because η_{p^+} and η_p that are two main components in η are improved by the intensity of the light injected form the p^+-side surface and therefore D^* increases.

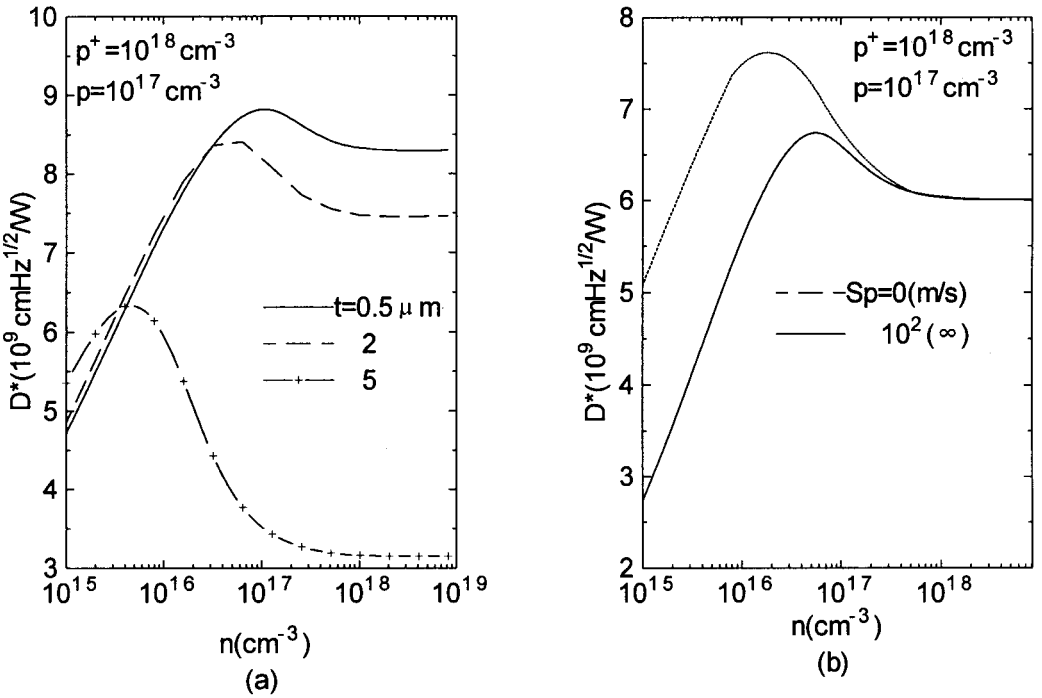

Fig. 4. The dependence of D^* on the n-side carrier concentration (n) with the n-side (a) width (t) and (b) surface recombination velocity (S_p) as parameters for the p^+–p–n structure in the backside illuminated case.

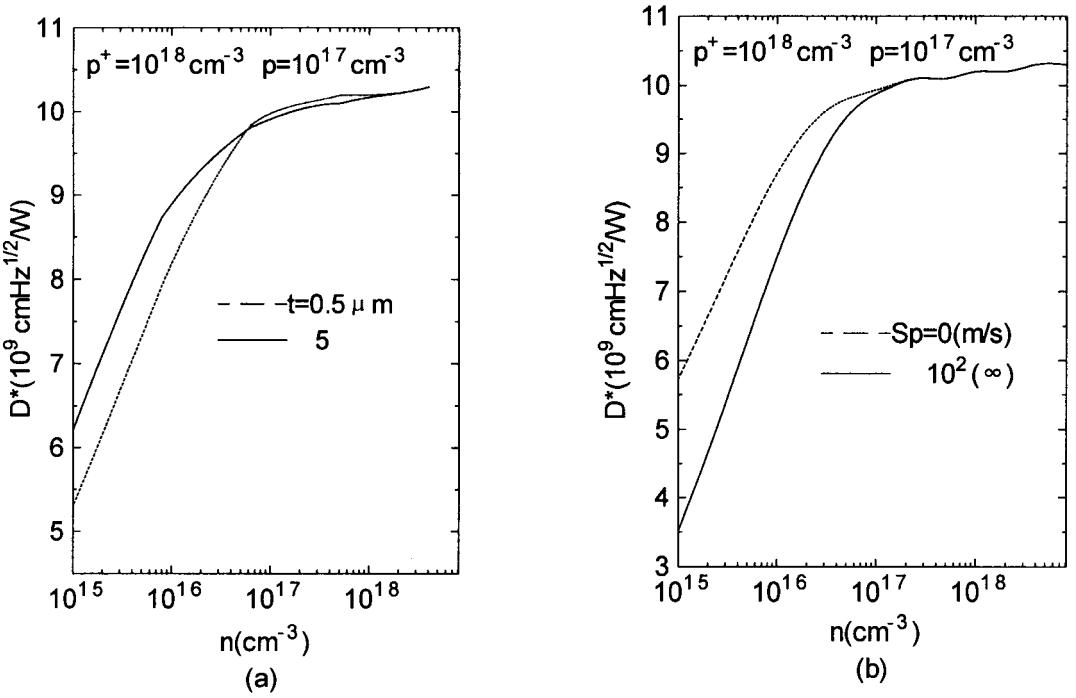

Fig. 5. The dependence of D^* on the n-side carrier concentration (n) with the n-side (a) width (t) and (b) surface recombination velocity (S_p) as parameters for the p^+–p–n structure in the frontside illuminated case.

3.2. The detectivity in an n^+–n–p structure

The quantum efficiency and its components in the frontside illuminated case are similar to those in Fig. 2. The light injected from the n^+-side surface decides that the quantum efficiency will be obviously influenced by the n^+-side parameters.

D^* in the frontside illuminated case is shown in Fig. 6 as a function of the n-side carrier concentration (n), with the n^+-side carrier concentration (n^+) and the width (t_{n^+}) as parameters respectively. In this case, D^* is determined by η and its shape is similar to η but not to R_0A. There is an interesting one in Fig. 6: with increasing n^+ and t_{n^+}, the value of D^* has a opposite change, from strongly going up to going down. This is an inevitable result due to the influence of η on D^*, in which η_{n^+} related with n^+ and t_{n^+} has much contribution. Moreover, the light injected form the n^+-side surface is first through the n^+ region so that the n^+-side width will affect not only the quantum efficiency in the n^+-side but also other region components. Although R_0A can not be influenced by the n^+-side width [13], D^* is clearly reduced by increasing t_{n^+} in Fig. 6(b). As the report in Ref. [13], R_0A in this structure is not affected by the n^+-side surface recombination velocity (S_p) because of $l_{np^+} \ll t_{n^+}$. Here we find that η is also not related with S_p, and thus D^* will not be changed by S_p.

For the frontside illuminated case, the quantum efficiency in the n region (η_n) is one of the contribution to η in $n < 10^{17}$ cm^{-3}. Thus the change of the n-side width (t) influences the quantum efficiency and therefore affects D^*. Fig. 7 shows the dependence of D^* on the n-side carrier concentration with t as a parameter, in the frontside illuminated case. D^* and its shape are controlled by η and lowering the n-side width will improve D^*, especially in $n > 10^{18}$ cm^{-3}, D^* markedly rises.

As the report for an n–p homojunction GaInAsSb infrared detector [10], D^* as a function of p-side carrier concentration is controlled by R_0A and its shape is similar to R_0A, but D^* is improved by increasing the p-side width, because η increases and reaches saturation. This changes the trend of D^* in the n^+–n–p structure also appears.

Fig. 8 shows the dependence of R_0A, η and D^* on the p-side width with the p-side surface recombination velocity (S_e) as a parameter, in the frontside illuminated case. The surface recombination velocity reduces R_0A, η and D^*, but η is much less sensitive to the p-side surface recombination velocity than R_0A and D^*, which can be found in Fig. 9. The shape of D^* is com-

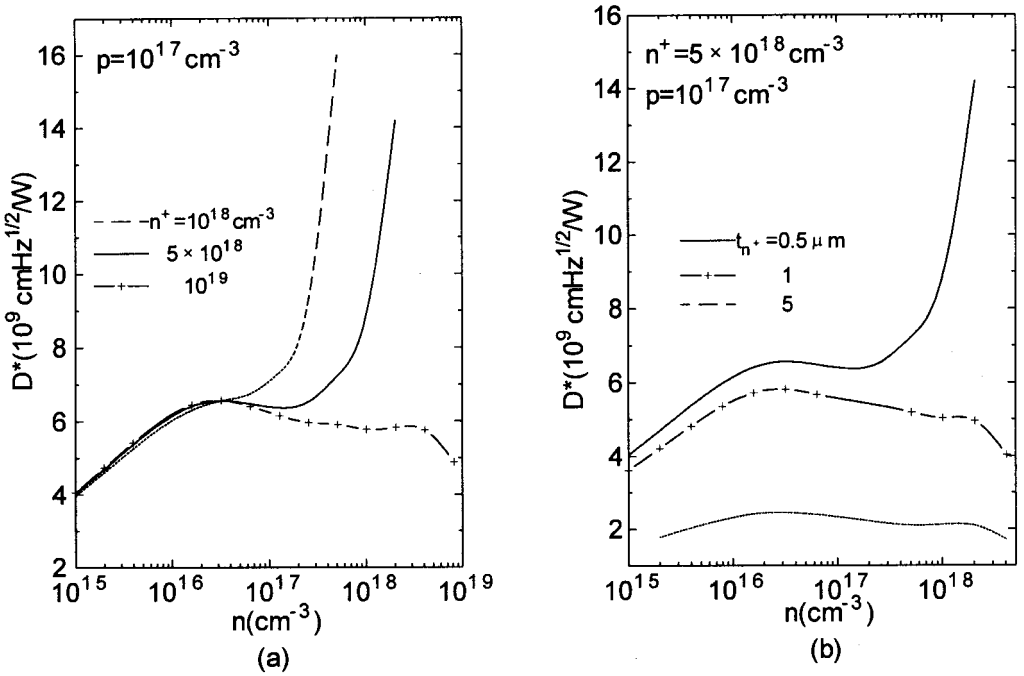

Fig. 6. The dependence of D^* on the n-side carrier concentration (n) with the n^+-side (a) carrier concentration (n^+) and (b) width (t_{n^+}) as parameters for the n^+–n–p structure in the frontside illuminated case.

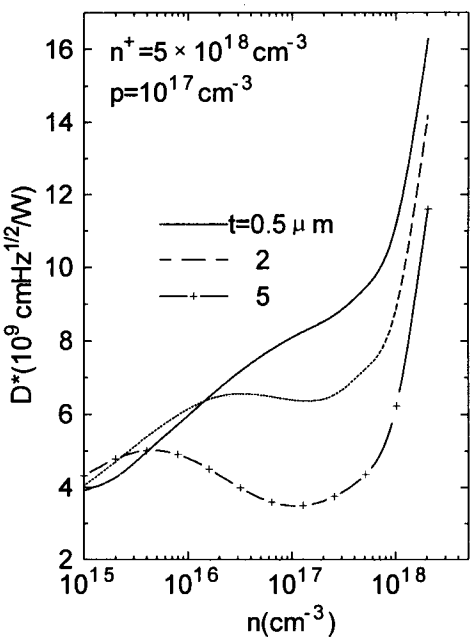

Fig. 7. The dependence of D^* on the n-side carrier concentration (n) with the n-side width (t) as a parameter for the n^+–n–p structure in the frontside illuminated case.

pletely different from these of R_0A and η. R_0A with the change of d first goes down at $S_e=0$, and little by little R_0A rises up as S_e increases. The quantum efficiency with the change of d rapidly increases and then saturates. D^* goes through a peak as d increases, further the peak moves to a higher d as the surface recombination increases. D^* can be separated into two parts at the point of the peak: D^* is determined by η before the peak and by R_0A after the peak, respectively.

In Fig. 9, R_0A and D^* in the backside illuminated case are plotted as a function of the n-side carrier concentration (n), with the n^+-side carrier concentration (n^+) as a parameter, under the condition of other parameters in Table 1 keeping constants. R_0A and D^* have the similar various trends, in which the peaks moves to high n with high n^+. In this case, D^* related with other parameters and its shape are also controlled by R_0A, which are similar to in Fig. 9(b). Unlike in the frontside illuminated case, η in the backside illuminated case is almost controlled by η_p, while η_{n^+} is too low to dedicate η, which induces that the parameters in the n^+-side can not influence η. Moreover, η_n and η_{dr} only have a little contribution to η through t in $n < 10^{17}$ cm^{-3}. But as shown in Fig. 9, the value of D^* is not optimum in $n < 10^{17}$ cm^{-3}. Therefore even

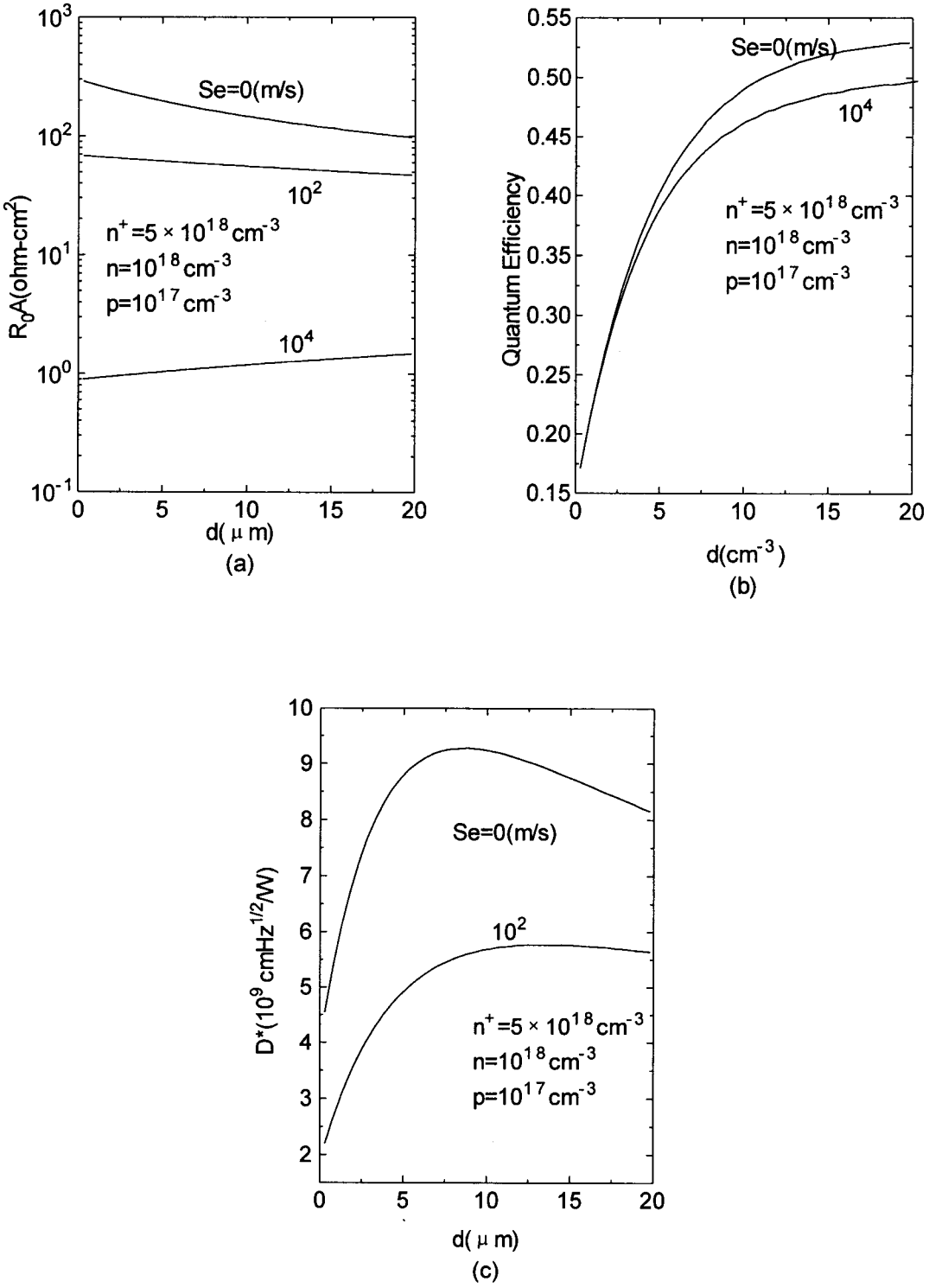

Fig. 8. The dependence of R_0A, η and D^* on the p-side width (d) with the p-side surface recombination velocity (S_e) as a parameter for the n^+–n–p structure in the frontside illuminated case.

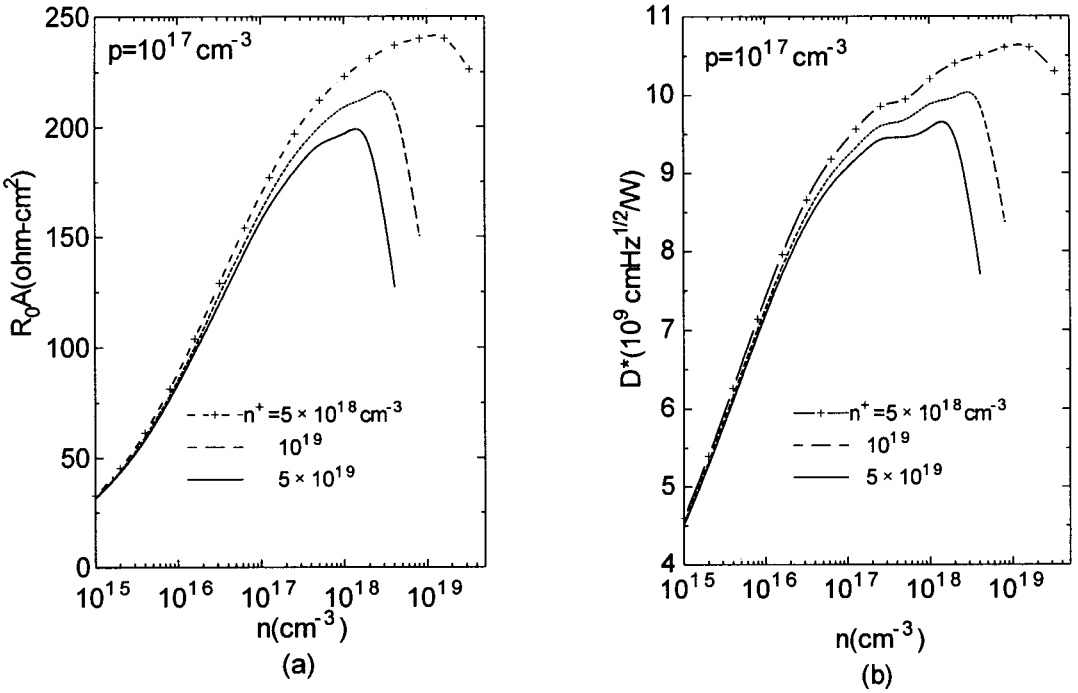

Fig. 9. The dependence of R_0A and D^* on the n-side carrier concentration with the n^+-side carrier concentration (n^+) as a parameter for the n^+–n–p structure in the backside illuminated case.

though the n-side width changes D^*, the optimum D^* cannot be obtained in that range.

As for the frontside illuminated case, D^* in the backside illuminated case appears a peak with the change of the p-side width (d). Fig. 10 shows D^* as a function of the p-side width (d), with the n^+- and n-side carrier concentrations as parameters, which are corresponding to the peak of D^* in Fig. 9. The value of the optimum D^* are at $d = 10$ μm or so. Moreover, high D^* will be obtained with high n^+ and n.

In order to find the optimum D^* with the material parameters in the different structures with different directions of the light injected, the values of D^* and the corresponding conditions and parameters are shown in Table 2. D^* in the frontside illuminated case is higher than that in the backside illuminated case, either for the n^+–n–p structure or for the p^+–p–n structure, because η_{n^+} in the frontside illuminated case is higher than the one in the backside illuminated case, which improves η and D^*.

Depending on these calculation, we know that D^* is much higher than those in the experimental reports [15,16]. Therefore these results are useful to improve the properties of GaInAsSb infrared detectors through the material growth and device fabrication.

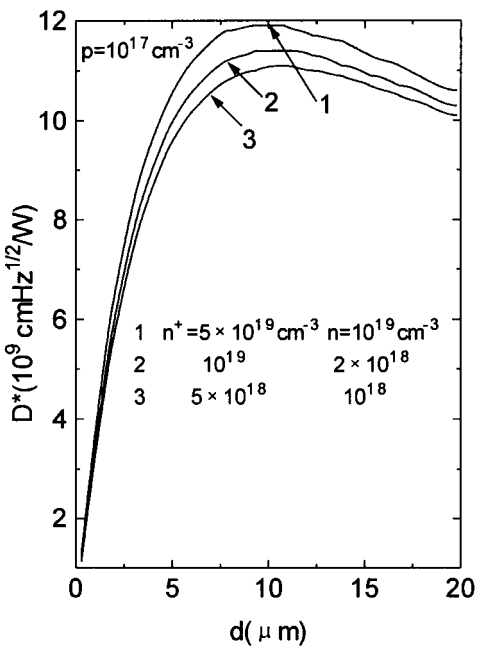

Fig. 10. The dependence of D^* on the p-side width (d) with the n^+- and n-side carrier concentrations as parameters for the n^+–n–p structure in the backside illuminated case.

Table 2
The optimum D^* and corresponding material parameters and the light injected direction

Basic parameters	T = 300 K, x = 0.8, λ = 2.5 μm, $N_f = 10^{14}$ cm^{-3}, $\sigma_s = 10^{-15}$ cm^{-3}; $\mu_{p+} = \mu_p$ = 240 cm^2/V s, $\mu_{n+} = \mu_n$ = 1000 cm^2/V s								
p^+–p–n structure	p^+ region parameters			p region parameters		n region parameters			D^* (cm Hz$^{1/2}$/W)
	p^+ (cm^{-3})	S_e (m/s)	d_{p^+} (μm)	p (cm^{-3})	d (μm)	n (cm^{-3})	S_p (m/s)	t (μm)	
$\xrightarrow{Light}p^+$–p–n	10^{18}	0	0.5	3.28×10^{17}	5	10^{18}	0	2	1.7×10^{10}
$\xrightarrow{Light}n$–p–p^+	10^{18}	0	0.5	6.55×10^{17}	5	10^{16}	0	2	1.15×10^{10}
n^+–n–p structure	n^+ region parameters			n region parameters		p region parameters			
	n^+ (cm^{-3})	S_p (m/s)	t_{n^+} (μm)	n (cm^{-3})	t (μm)	p (cm^{-3})	S_e (m/s)	d (μm)	
$\xrightarrow{Light}n^+$–n–p	5×10^{18}	0	0.5	2.05×10^{18}	0.5	10^{17}	0	5	1.63×10^{10}
$\xrightarrow{Light}p$–n–n^+	5×10^{19}	0	0.5	10^{19}	2	10^{17}	0	8.8–10.8	1.19×10^{10}

4. Conclusion

In this paper, the numerical analysis of the detectivity in the p^+–p–n and n^+–n–p structure $Ga_{0.8}In_{0.2}As_{0.81}Sb_{0.19}$ infrared detectors are performed, based on the material parameters and the direction of the injected light. The behavior of D^* is influenced by the R_0A and the quantum efficiency. The conclusions are drawn as follows.

1. The high D^* is obtained with the light incident from the surface of the heavily-doped layer.
2. The surface recombination velocity in the p-type material is one of the most important parameter to effect D^*. The higher surface recombination velocity is, the lower D^* is.
3. The values of parameters in the heavily-doped layer are important to affect D^*. In the p^+–p–n structure, lowering the parameters in the p^+-side will effectively improve D^*, in which it is not related with the direction of the incident light. However, in the n^+–n–p structure, except for the surface recombination velocity of the n^+-side that does not change D^*, D^* in the frontside illuminated case requires the low value of the parameters in the n^+-side, while in the backside illuminated case, the high n^+-side carrier concentration is useful to improve D^* and the n^+-side width does not affect D^*.
4. For the p^+–p–n structure, except that D^* in the frontside illuminated case varies with the n-side carrier concentration in a way that is similar to that of R_0A, D^* is dominated by the quantum efficiency in other conditions.
5. For the n^+–n–p structure, in the frontside illuminated case, D^* with the variety of the n-side carrier concentration is controlled by the quantum efficiency, while D^* with the variety of the p-side carrier concentration is dominated by R_0A. However in the backside illuminated case, D^* is controlled by R_0A either with the variety of the p-side carrier concentration or with that of the n-side carrier concentration.
6. The p-side width (d) in the different structures has different influences on D^*. For the p^+–p–n structure, lowering d in the higher p-side carrier concentration ($p > 10^{17}$ cm^{-3}) will improve D^*. However for the n^+–n–p structure, an optimum d can obtain the best D^*.

Acknowledgements

This paper is supported by the National Advanced Materials Committee of China (NAMCC).

References

[1] Hasenberg TC, Miles RH, Kost AR, West L. IEEE J Quantum Electron 1997;33(18):1403–6.
[2] Shin J, Hsu Y, Hsu TC, Stringfellow GB. J Electron Mater 1995;24(11):1563–9.
[3] Aardvark A, Allogho GG, Bougnot G, David JPR, Giani A, Haywood SK, Hill G, Klipstein PC, Mansoor F, Mason NJ, Nicholas RJ, Pascal-Delannoy F, Pate M, Ponnampalam L, Walker PJ. Semicond Sci Technol 1993;8(1S):S380.
[4] Srivastava AK, Dewinter JC, Caneau C, Pollack MA, Zyskind JL. Appl Phys Lett 1986;48(14):903.
[5] France PW, Carter SF, Moore MW, Williams JR. SPIE 1986;618:51.
[6] Baranov AN, Imenkov AN, Sherstnev VV, Yakovlev YuP. Appl Phys Lett 1994;64:2480–2.

[7] Mikhailova MP, Titkov AN. Semicond Sci Technol 1994;9:1279–95.
[8] Mishurnyi VA, Anda de F, Gorbatchev AYu, Vasil'ev VI, Faleev NN. J Crystal Growth 1997;180:34–9.
[9] Tian Y, Zhou T, Zhang B, Jin Y, Ning Y, Jiang H, Yuang G. Opt Eng 1998;37:1754–62.
[10] Tian Y, Zhou T, Zhang B, Jin Y, Jiang H. J Phys D 1998;31:3291–7.
[11] Hauser J, Dunbar P. Solid-State Electron 1975;18:715.
[12] Alamo J, Meerbergen J, D'Hoor F, Nijs J. Solid-State Electron 1981;24:533.
[13] Tian Y, Zhang B, Zhou T, Jin Y, Jiang H, (submitted).
[14] Dhar V, Ashokan R. Semicond Sci Technol 1997;12:580–8.
[15] Yan S, Zhang JH, Lee H, Sarathy J, Cohen M, Olsen G. Electron Lett 1996;32(24):2268–9.
[16] Zhang B, Zhou T, Jiang H, Ning Y, Jin Y. Electron Lett 1995;31:830–1.